Structural Changes of the Prion Protein in Lipid Membranes Leading to Aggregation and Fibrillization†

Jurate Kazlauskaite,‡ Narinder Sanghera,‡,§ Ian Sylvester,‡,§ Catherine Vénien-Bryan,|| and Teresa J. T. Pinheiro*,‡

Department of Biological Sciences, University of Warwick, Gibbet Hill Road, Coventry CV4 7AL, United Kingdom, and Laboratory of Molecular Biophysics, University of Oxford, South Parks Road, Oxford OX1 3QU, United Kingdom

Received September 19, 2002; Revised Manuscript Received December 19, 2002

ABSTRACT: Prion diseases are associated with a major refolding event of the normal cellular prion protein, PrP^C, where the predominantly α-helical and random coil structure of PrP^C is converted into a β-sheet-rich aggregated form, PrP^{Sc}. Under normal physiological conditions PrP^C is attached to the outer leaflet of the plasma membrane via a GPI anchor, and it is plausible that an interaction between PrP and lipid membranes could be involved in the conversion of PrP^C into PrP^{Sc}. Recombinant PrP can be refolded into an α-helical structure, designated α-PrP isoform, or into β-sheet-rich states, designated β-PrP isoform. The current study investigates the binding of β-PrP to model lipid membranes and compares the structural changes in α- and β-PrP induced upon membrane binding. β-PrP binds to negatively charged POPG membranes and to raft membranes composed of DPPC, cholesterol, and sphingomyelin. Binding of β-PrP to raft membranes results in substantial unfolding of β-PrP. This membrane-associated largely unfolded state of PrP is slowly converted into fibrils. In contrast, β-PrP and α-PrP gain structure with POPG membranes, which instead leads to amorphous aggregates. Furthermore, binding of β-PrP to POPG has a disruptive effect on the integrity of the lipid bilayer, leading to total release of vesicle contents, whereas raft vesicles are not destabilized upon binding of β-PrP.

Prion diseases are associated with the conversion of the benign cellular form of the prion protein (PrP^C)[1] into an infectious scrapie isoform (PrP^{Sc}) (*1*). There are no detectable chemical differences between PrP^C and PrP^{Sc}. A large body of experimental evidence indicates that the fundamental difference between the two forms of PrP resides in their conformation, which results in considerable differences in their physicochemical properties. PrP^C is rich in α-helical structure, monomeric and susceptible to enzyme digestion. In contrast, PrP^{Sc} has a large content of β-sheet, forms highly insoluble aggregates, and is partially resistant to proteolytic digestion (*2*, *3*). It is apparent that a major refolding event underlying the conversion of PrP^C into PrP^{Sc} plays a key role in the pathogenesis of prion diseases (*4*). However, the molecular details of this conformational transition are not clearly understood.

Recombinant prion proteins can be refolded *in vitro* into different conformations, designated PrP isoforms. Refolding under oxidizing conditions yields a predominantly α-helical conformation representing PrP^C, whereas reducing conditions result in conformations with higher β-sheet content (*5*, *6*). Whereas the α-helical isoform is monomeric and susceptible to enzyme digestion, β-sheet isoforms are oligomeric, partially resistant to proteolytic digestion, and form insoluble amorphous aggregates and fibrils (*7*, *8*). Thus, recombinant β-sheet forms of PrP have properties of intermediate conformations of PrP that lead to PrP^{Sc}. The availability of such *in vitro* isoforms of PrP have prompted the design of experiments *in vitro* to decipher the underlying structural events in PrP conversion (*6*, *8*, *9*−*11*). However, to date most of these studies have only been carried out in solution whereas PrP is a cell-surface glycoprotein attached to the plasma membrane surface via a GPI anchor.

Several experimental observations (*12*−*15*) suggest that an interaction of PrP with the membrane surface may play a role in the conversion of PrP^C into PrP^{Sc}. In particular, the fact that PrP^C is released from the cell surface after digestion with phosphatidylinositol-specific phospholipase C, and PrP^{Sc} is not after similar treatment (*13*, *14*), strongly supports the idea that an altered membrane association of PrP may be an important factor in the mechanism of prion diseases. Also, during its biogenesis PrP can be produced in alternative topological forms (*16*). A secretory form fully translocated through the ER lumen is the precursor of the GPI-anchored molecule, and a second transmembrane form of two topolo-

† This work has been supported by the Medical Research Council (G9901445), the Wellcome Trust (SHoWCAse 053914/Z/98/Z)), the Biotechnology and Biological Sciences Research Council (N.S. studentship), and the Royal Society. T.J.T.P. is a Royal Society University Research Fellow.

* To whom correspondence should be addressed. Tel: +44 24 7652 8364. Fax: +44 24 7652 3701. E-mail: t.pinheiro@warwick.ac.uk.

‡ University of Warwick.

§ Current addresses: Accentus plc, Biologics, Cowley, Oxford OX4 6LY, U.K. (N.S.); Institute for Animal Health, Compton, Newbury, Berks. RG20 7NN, U.K. (I.S.).

|| University of Oxford.

[1] Abbreviations: ATR FTIR, attenuated total reflection Fourier transform infrared; CD, circular dichroism; chol, cholesterol; DPPC, dipalmitoylphosphatidylcholine (1,2-dipalmitoyl-*sn*-glycero-3-phosphocholine); EM, electron microscopy; POPC, palmitoyloleoylphosphatidylcholine (1-palmitoyl-2-oleoyl-*sn*-glycero-3-phosphocholine); POPG, palmitoyloleoylphosphatidylglycerol [1-palmitoyl-2-oleoyl-*sn*-glycero-3-phospho-*rac*-(1-glycerol)]; PrP, prion protein; NMR, nuclear magnetic resonance; SHaPrP, Syrian hamster prion protein; SM, sphingomyelin.

10.1021/bi026872q CCC: $25.00
Published on Web 03/01/2003

gies (amino or carboxyl terminus in the lumen) associated with the ER membrane.

Like other GPI-anchored proteins, PrP^C is segregated into cholesterol and sphingomyelin-rich domains or lipid rafts in the plasma membrane (*17*−*19*) from where its metabolic fate is determined. From the plasma membrane PrP^C can be recycled, degraded, or possibly converted into PrP^{Sc}. The subcellular site for the formation of PrP^{Sc} is unknown; however, conversion occurs after PrP^C reaches the plasma membrane (*20*, *21*). A recent study of PrP conversion in a cell-free system utilizing purified raft membranes showed that conversion of raft-associated GPI-anchored PrP^C to PrP^{Sc} requires insertion of PrP^{Sc} into the lipid membrane (*22*). Evidence from scrapie-infected cultured cells implicates the plasma membrane and endocytic organelles as relevant sites, but it is unclear which provides a more favorable environment for conversion and whether compartments along the secretory pathway might also be involved. Once PrP^{Sc} is formed, it appears to accumulate in late endosomes and lysosomes and on the cell surface (*19*, *23*, *24*) or in extracellular spaces in the form of amorphous deposits, diffuse fibrils, or dense amyloid plaques (*25*). Thus, it seems plausible that either at the plasma membrane or in the endosomal/lysosomal pathway an interaction of PrP with lipid membranes could feature in the mechanism of prion conversion.

The observed multiplicity of PrP conformations *in vitro* under different conditions suggests that within the cell as PrP experiences various subcellular environments during trafficking in the ER, at the plasma membrane and recycling through the endocytic pathway, PrP may exist in different conformations. In addition, in these various cellular environments PrP is associated with lipid membranes. Thus, the potential role of an interaction of PrP with membranes in PrP conversion could happen in two ways: first, a direct involvement in the conversion mechanism, whereby a PrP^C interaction with the membrane surface drives the structural changes that lead to the formation of PrP^{Sc}; alternatively, due to external environmental changes at the various membrane locations, PrP^C could undergo a structural change to other PrP^{Sc}-like conformations, which may have higher affinity to lipid membranes and be on the pathway of conversion to PrP^{Sc}. Thus, it is important to study the binding of prion isoforms to lipid membranes and their structural properties in association with membranes.

In a previous study (*26*) we have investigated the binding of the α-PrP isoform of the Syrian hamster prion protein domain SHaPrP(90−231) to model lipid membranes. We showed that α-PrP binds to negatively charged lipid membranes of POPG and to zwitterionic membrane vesicles of DPPC and model raft membrane vesicles composed of DPPC, cholesterol, and sphingomyelin. The binding of α-PrP to POPG membranes involves both electrostatic and hydrophobic lipid−protein interactions and results in partial insertion of PrP into the lipid bilayer. This membrane-associated conformation of α-PrP is richer in β-sheet structure and has a disruptive effect on the integrity of the lipid bilayer, leading to total release of vesicle contents. In contrast, binding to raft membranes results in a conformation of α-PrP with high content of α-helical structure, which does not destabilize the lipid bilayer.

In the current study we investigate the binding of β-PrP to lipid membranes, compare the structural properties of α- and β-PrP associated with lipid membranes, and study their propensities to aggregation and fibrillization in membranes. As in the studies with α-PrP, measurements were carried at pH 7 to represent the pH surrounding the plasma membrane and at pH 5 to model the acidic environment of endocytic vesicles. We found that β-PrP has a higher affinity to POPG membranes at pH 5 than at pH 7, unlike α-PrP which binds strongly at both pH values. β-PrP also binds to raft membranes at both pH 7 and pH 5, whereas α-PrP binds only at pH 7. Binding of β-PrP to POPG membranes results in an increase in β-sheet structure and release of vesicle contents, whereas binding of β-PrP to raft membranes results in substantial unfolding of β-PrP without destabilizing the integrity of vesicles. Binding of α- or β-PrP to POPG membranes results in protein aggregation, whereas, with raft membranes, no aggregation is detected for α-PrP, but binding of β-PrP results in PrP fibrillization.

EXPERIMENTAL PROCEDURES

Materials. Cholesterol, POPC, POPG, and sphingomyelin were purchased from Avanti Polar Lipids, Inc. (Alabaster, AL). DPPC was from Sigma-Aldrich (Dorset, U.K.).

Expression, Purification, and Refolding of α-PrP and β-PrP. Syrian hamster recombinant prion protein SHaPrP-(90−231) was expressed using an alkaline phosphatase promotor in a protease-deficient strain of *Escherichia coli* (27C7) as described previously (*27*). The prion protein accumulates as insoluble aggregates in the periplasmic space. From these inclusion bodies PrP can be refolded to a predominantly α-helical conformation (α-PrP) or to a state with a higher content of β-sheet structure (β-PrP), depending on whether refolding is carried out under oxidizing or reducing conditions, respectively (*5*, *27*). Purification of α-PrP was carried out as described in Sanghera and Pinheiro (*26*). The preparation of β-PrP followed the method described for α-PrP, but keeping all protein purification steps from the extraction from inclusion bodies under stringent reducing conditions with all buffers containing a large excess of DTT (20−100 mM). The purity of the final product was determined by SDS−polyacrylamide gel electrophoresis and electrospray ionization mass spectrometry. Purified PrP was dialyzed against 5 mM MES, pH 5.5, and stored in small aliquots. Protein samples were thawed prior to measurements and used on the same day, unless stated otherwise. PrP concentration was determined spectrophotometrically using a molar extinction coefficient ϵ_{280} of 24420 M^{-1} cm^{-1} (*28*).

Lipid Vesicles. Small unilamellar lipid vesicles were prepared by hydrating the required amount of dried lipid with the desired buffer: 20 mM sodium phosphate, pH 7.2, 20 mM sodium acetate buffer, pH 5.0, or 5 mM MES, pH 5. Buffers were deoxygenated with nitrogen gas, and the hydrated lipids were maintained under a nitrogen atmosphere. Phospholipids in chloroform solutions were dried under a rotary evaporator, and the resulting lipid film was left under vacuum overnight to remove all traces of organic solvent. For the preparations of mixed lipid membranes, lipids were codissolved in chloroform or chloroform/methanol, and a lipid film formed as described above. After lipid hydration the resulting multilamellar liposome suspension was soni-

cated in a bath sonicator until a clear suspension of small unilamellar vesicles was obtained (typically 6.5 h periods). These preparations have been shown to yield vesicles with diameters ranging from 300 to 600 Å (*29*).

Binding of β-PrP to Lipid Membranes. Binding of β-PrP to various lipid vesicles was studied at pH 7 and 5 at 20 °C by monitoring the shift in λ_{max} of protein fluorescence upon addition of increasing amounts of lipid. For measurements at pH 7 vesicles were prepared in 20 mM sodium phosphate buffer, pH 7.2, whereas for measurements at pH 5 vesicles were in 20 mM sodium acetate buffer, pH 5.0. The protein concentration was kept constant at 5 μM and the lipid concentration varied from 5 μM to 10 mM, with exception of the binding measurements with DPPC/chol/SM membranes. Because of the higher light scattering levels with these vesicles, binding was measured on samples containing 2 μM PrP and the lipid concentration varied from 2 μM to 4 mM. Lipid/protein samples were prepared by adding 1 part of protein solution in 5 mM MES buffer, pH 5.5, to an equal volume of lipid vesicles at pH 7.2 or 5.0, resulting in a final pH of the lipid/protein samples of ∼7 and ∼5, respectively. Lipid/protein samples were mixed thoroughly and equilibrated for 2−3 min before fluorescence spectra were recorded on a Photon Technology International spectrofluorometer. Quartz cells of 4 mm and 1 cm path length were used with an excitation wavelength at 295 nm (2 nm bandwidth). Emission spectra were recorded from 300 to 450 nm (2 nm bandwidth), and typically, four scans were averaged per spectrum. The corresponding appropriate backgrounds (buffer for protein solutions or lipid alone at corresponding concentrations for lipid−protein samples) were subtracted from the final spectra.

Calcein Release. Lipid vesicles loaded with calcein (Molecular Probes, Oregon, OR) in their interior aqueous core were prepared as described previously (*26*) and used on the day of preparation.

The release of calcein from lipid vesicles upon binding of β-PrP was monitored by calcein fluorescence at 512 nm over a time scale of 500 s after 5 parts of lipid vesicles was manually mixed with 1 part of protein solution (5:1 v/v). The excitation wavelength was 490 nm, and both the excitation and emission slits were set to 1 nm. Experiments were performed at 20 °C. Release of calcein to the external medium leads to an increase in fluorescence caused by calcein dilution and consequent relief of self-quenching. The lipid concentration was 100 μM (single lipid membranes) and 1 mM (mixed lipid membranes), and protein concentrations varied from 10 to 500 nM. The fraction of calcein release (R_f) was calculated as described previously (*26*).

Circular Dichroism. Far-UV (185−260 nm) CD spectra were measured on a JASCO J-715 spectropolarimeter using 1 mm path length quartz cells. Typically, a scanning rate of 100 nm/min, a time constant of 1 s, a bandwidth of 1.0 nm, and a resolution of 0.5 nm were used. Spectra were measured at 20 ± 0.2 °C on samples containing 5−10 μM PrP alone or with freshly sonicated lipid vesicles. Normally, 16 scans were averaged per spectrum. The corresponding appropriate backgrounds (buffer for protein solutions or lipid alone at corresponding concentrations for lipid−protein samples) were subtracted from the final spectra.

ATR FTIR. Attenuated total reflection (ATR) Fourier transform infrared (FTIR) spectra were recorded at room temperature on a Bruker Vector 22 infrared spectrometer equipped with a liquid nitrogen-cooled mercury cadmium telluride (MCT) detector at a nominal resolution of 2 cm^{-1} in the range 1000−4000 cm^{-1}. The spectrometer was continuously purged with dried air (Jun-Air 600, Kent, U.K.) to minimize the spectral contribution of atmospheric water. Residual water vapor peaks were subtracted using reference spectra and baseline correction applied when necessary. The internal reflection element was a germanium ATR plate (50 × 20 × 2 mm) with an aperture angle of 45° yielding 25 internal reflections. Lipid−protein samples were prepared by the addition of an aliquot of a stock solution of β-PrP in 5 mM MES buffer, pH 5.5, to preformed lipid vesicles in 5 mM MES buffer, pH 5 or 7. Samples normally contained 10 μM PrP and 0.1−10 mM lipid. An aliquot of 40−60 μL was deposited on the ATR plate. Thin films of hydrated multibilayers of lipid containing PrP were obtained by slowly evaporating the excess water under a stream of N_2 gas. This procedure results in stacks of orientated bilayers with the lipid acyl chains approximately perpendicular to the surface of the plate (*30*). Protein films without lipids were prepared in a similar manner from their buffer solutions. Typically, the final spectrum is an average of 128 scans, corrected for the background using a clean germanium plate.

ATR FTIR spectra of deuterated samples were collected to aid the analysis of protein secondary structure (*31*, *32*). Deposited films on the ATR plate, prepared from samples in H_2O, were subjected to a stream of ^2H_2O-saturated N_2 gas for 30 min at room temperature. Peak fitting of the amide I band (1600−1700 cm^{-1}) was performed on nondeconvoluted spectra using GRAMS 32/AI software (Thermogalactic). Best fits to the experimental spectra were obtained with a Lorentzian line shape with a full width at half-height of 5−6 cm^{-1}. Band assignments were made according to Cabiaux et al. (*33*), helped by second derivative analysis of the FTIR spectra.

Electron Microscopy. Protein and vesicle−protein samples were prepared as described above and incubated at 25 °C for 21 days (buffers contained azide). After incubation samples were diluted to a protein concentration ∼50 μg/mL and applied to electron microscope grids coated with carbon film and stained with 2% uranyl acetate. The preparations were examined using a Philips CM120 electron microscope with an accelerated voltage of 100 kV. Electron micrographs were taken at a magnification of 45000 under low dose conditions.

RESULTS

Refolding of PrP. Recombinant PrP(90−231) can be refolded from *E. coli* inclusion bodies either as an α-helical conformation (α-PrP) or as a state with a higher content of β-sheet structure (β-PrP). Refolding under oxidizing conditions yields the α-PrP isoform which shows a characteristic far-UV CD spectrum with well-defined minima at 208 and 222 nm (Figure 1A) and a FTIR spectrum with a predominant amide I band at ∼1656 cm^{-1} (Figure 1B). In contrast, refolding of PrP(90−231) under reducing conditions produces a β-PrP isoform which has a far-UV CD spectrum with a minimum at ∼218 nm (Figure 1A) and an intense amide I band at ∼1626 cm^{-1} (Figure 1B), which are spectral signatures of β-sheet structure. Mass spectrometry showed

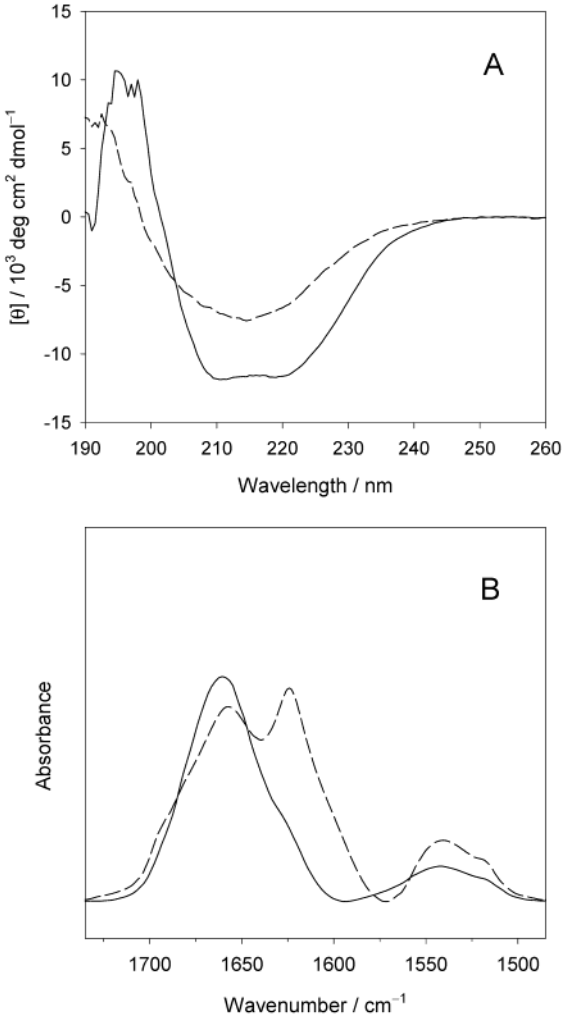

FIGURE 1: α- and β-isoforms of PrP(90−231) refolded from *E. coli* inclusion bodies. (A) Far-UV CD and (B) ATR FTIR spectra of α-PrP (solid line) and β-PrP (dashed line). CD spectra were recorded on samples containing 10 μM PrP in 20 mM sodium acetate buffer, pH 5; for FTIR spectra 50 μL of a 10 μM solution of PrP in 2 mM MES buffer, pH 5, was deposited on the ATR crystal and excess liquid evaporated under a N_2 stream.

that the two cysteines in α-PrP (Cys 179 and 214) are oxidized (i.e., forming a disulfide bond), whereas in β-PrP these cysteines are reduced, in agreement with previous results (*5*, *27*). Analytical ultracentrifugation (AUC) results showed that α-PrP is a monomeric protein in solution, whereas β-PrP tends to aggregate into large oligomeric states during AUC measurements (data not shown). These results are in agreement with previous reports showing that PrP under reducing conditions adopts diverse conformations and oligomeric states, with the proportion and occurrence of the various sates depending on the experimental conditions (*6*, *8*, *9*).

Binding of β-PrP to Lipid Membranes. Intrinsic protein fluorescence has been used to monitor the binding of α-PrP to lipid membranes (*26*). The prion protein PrP(90−231) has two Trp residues at positions 99 and 145, which dominate the fluorescence of PrP. The fluorescence spectrum of β-PrP in solution has a maximum intensity at 344 nm (pH 5) or 341 nm (pH 7) (λ_{max}), which is consistent with a relatively polar environment of the tryptophan residues. Binding of proteins to lipid vesicles is normally accompanied by a blue

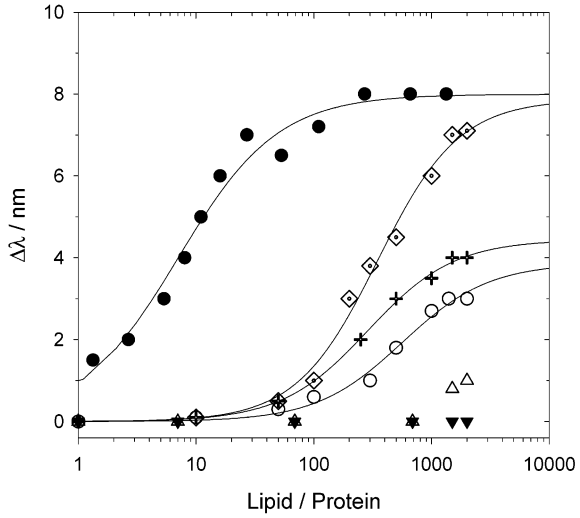

FIGURE 2: Binding of β-PrP to lipid membranes. The blue shift (Δλ) of the fluorescence maximum for PrP with membranes of POPG at pH 7 (open circles) and pH 5 (filled circles), POPC at pH 7 (open triangles) and pH 5 (filled triangles), and raft membranes of DPPC/chol/SM at pH 7 (crosses) and pH 5 (diamonds) is represented as a function of lipid concentration. Protein concentration was kept constant and the lipid-to-protein ratio is in molar ratio. The blue shift (difference between λ_{max} for PrP in solution and λ_{max} for PrP with lipid) was measured from Trp fluorescence spectra recorded at 20 °C and using an excitation wavelength at 295 nm.

shift of the protein fluorescence λ_{max} and an increase in fluorescence intensity. We have used this approach to investigate the binding of β-PrP to several model lipid membranes, containing either a single type of lipid or mixtures of different lipids. We found that β-PrP binds to negatively charged lipid membranes of POPG and to model raft membranes composed of DPPC, cholesterol (chol), and sphingomyelin (SM) (DPPC/chol/SM, 50:30:20, molar ratio) (Figure 2). Binding of β-PrP to POPG and raft membranes is accompanied by a similar blue shift in the λ_{max} at binding saturation level for a given pH (∼8 nm for pH 5 and ∼4 nm for pH 7; Figure 2). The fluorescence results also showed that β-PrP does not bind to zwitterionic lipid vesicles of POPC at either pH 7 or pH 5 (Figure 2).

Membrane Destabilization. To investigate whether β-PrP has a destabilizing effect on membranes, we have measured the release of calcein from lipid vesicles upon binding of β-PrP (Figure 3). This approach has been widely used to characterize the extent of perturbation to membranes exerted by bound proteins (*34*, *35*) and peptides (*36*). The results show that β-PrP destabilizes POPG membranes, both at pH 7 and at pH 5. Binding of β-PrP to POPG membranes induces a release of ∼80% of calcein from loaded vesicles for PrP concentrations equal and above 300 nM. In contrast, raft-like membranes retain their calcein content upon binding of β-PrP.

Structural Changes in β-PrP upon Association with Lipid Membranes. ATR FTIR was used to investigate the structural changes on β-PrP occurring upon interaction with lipid membranes both at pH 5 and at pH 7. Typical ATR FTIR spectra of PrP in the absence and presence of different lipid membranes are presented in Figure 4. These spectra show the amide I and amide II bands between 1700 and 1600 cm^{-1} and 1580−1510 cm^{-1}, respectively, arising from C═O

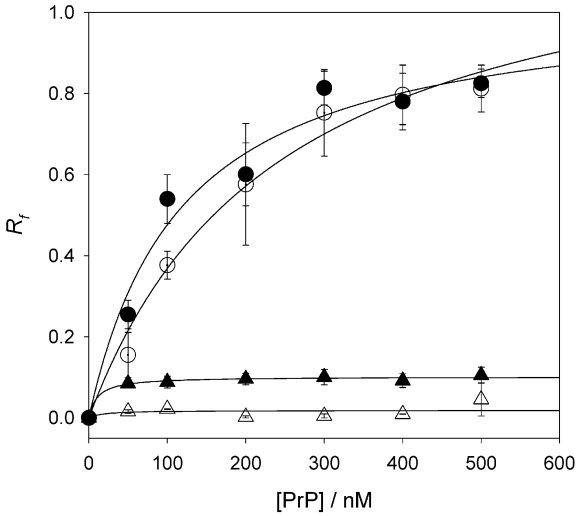

FIGURE 3: Summary of the extent of calcein release from various lipid membranes induced by β-PrP. Calcein release from lipid vesicles of POPG (circles) and raft-like vesicles of DPPC/chol/SM (triangles) at pH 5 (filled symbols) and pH 7 (open symbols). Calcein release (R_f) is represented as a fraction of total release upon detergent solubilization of vesicles. Data points are the mean value of two measurements on separate samples. Lines are for guidance only and have no theoretical significance.

stretching and N−H bending and stretching vibrations of the protein peptide group. For protein−lipid samples a band at ~1740 cm^{-1}, arising from the lipid ester carbonyl stretching vibration, is also present. The FTIR spectrum of β-PrP in solution exhibits an amide I band with a maximum absorption at ~1656 cm^{-1} associated with α-helical structure and a pronounced component at ~1626 cm^{-1}, characteristic of β-sheet structure. Binding of β-PrP to POPG and raft-like membranes was accompanied by an increase of the intensity of the amide I band at ~1656 cm^{-1} both at pH 5 and at pH 7 (Figure 4). The increase of the intensity under 1656 cm^{-1} is associated with an increase in α-helical structure and/or random coil. Far-UV CD of β-PrP with POPG vesicles show defined minima at 208 and 222 nm, typical of CD spectra for proteins with predominant α-helical structure (Figure 5A,B). At pH 7, β-PrP is converted to a α-helical-enriched form for all lipid concentrations studied (Figure 5A), whereas at pH 5 a different protein conformation is formed at low lipid concentration (Figure 5B). With raft membranes a smaller increase in the intensity of the bands at 208 and 222 nm is observed (Figure 5C). Instead, broader CD spectra of β-PrP with raft membranes are obtained, which may be associated with an increase in the negative band at ~200 nm characteristic of random coil.

Because the random coil contribution under the amide I band falls within very similar wavenumbers of the α-helix band, deuteration of samples is normally employed to distinguish between α-helical and random coil components. Usually, a brief period (a few minutes) of $H_2O/^2H_2O$ exchange is sufficient to shift the random coil band to lower wavenumbers away from the α-helix band (*31*). Figure 6 shows the FTIR spectra of β-PrP with POPG and raft membranes in H_2O and after $H_2O/^2H_2O$ exchange. Whereas for β-PrP with raft membranes a large component under the amide I moves within the limits of random coil (Figure 6A), with POPG a large fraction of the amide I intensity remains

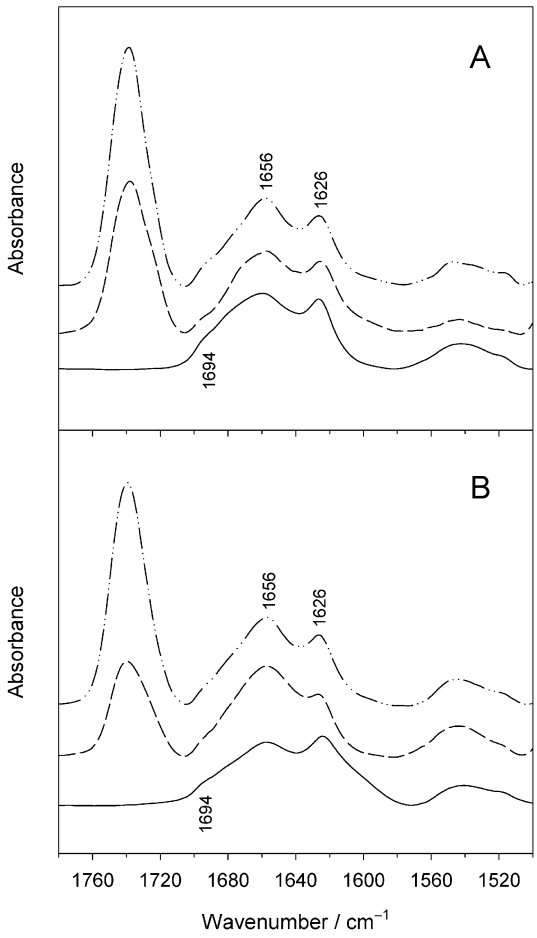

FIGURE 4: Structural changes of β-PrP with lipid membranes detected by FTIR. Representative ATR FTIR spectra of β-PrP alone (solid line) and with model raft membranes composed of DPPC/chol/SM (50:30:20, molar ratio) (dashed line) and single lipid membranes of POPG (dash-dot-dot line) at pH 7 (A) and pH 5 (B). The amide I bands are normalized to a constant area. Typically, films contained 10 μg of protein and ~154 μg of lipid (lipid-to-protein molar ratio ~176:1), and samples were prepared in 5 mM sodium phosphate buffer, pH 7, or 5 mM MES, pH 5.

within the α-helical region (Figure 6B). This interpretation is further illustrated by the fitted peaks shown in Figure 6.

Peak fitting analysis of the amide I band was employed to quantitatively analyze the main structural changes of β-PrP and α-PrP upon binding to lipid membranes. Analysis of the amide I band revealed that α-PrP has 37% α-helix, 22% random coil, and 9.5% β-sheet, in good agreement with the NMR structure (*37*), whereas β-PrP has a lower content of α-helical structure (21%) and a high content (35%) of β-sheet (Table 1). Overall, the secondary structure content of β-PrP is analogous to the secondary structure of the proteinase K-resistant core of PrP extracted from tissues of diseased animals (Table 1). Binding of β-PrP to POPG membranes results in an 11% increase in random coil and 8% gain in β-sheet structure, whereas binding of β-PrP to raft membranes results in a reduction of β-sheet and turns and a large increase in random coil (from 4% in solution to 39% with raft membranes) with no change in α-helix content (Table 1). In contrast, with POPG membranes α-PrP gains α-helix (an increase from 37% in solution to 50% with lipid) and β-sheet structure (from 9.5% to 20%) using all random coil present in α-PrP in solution (Table 1).

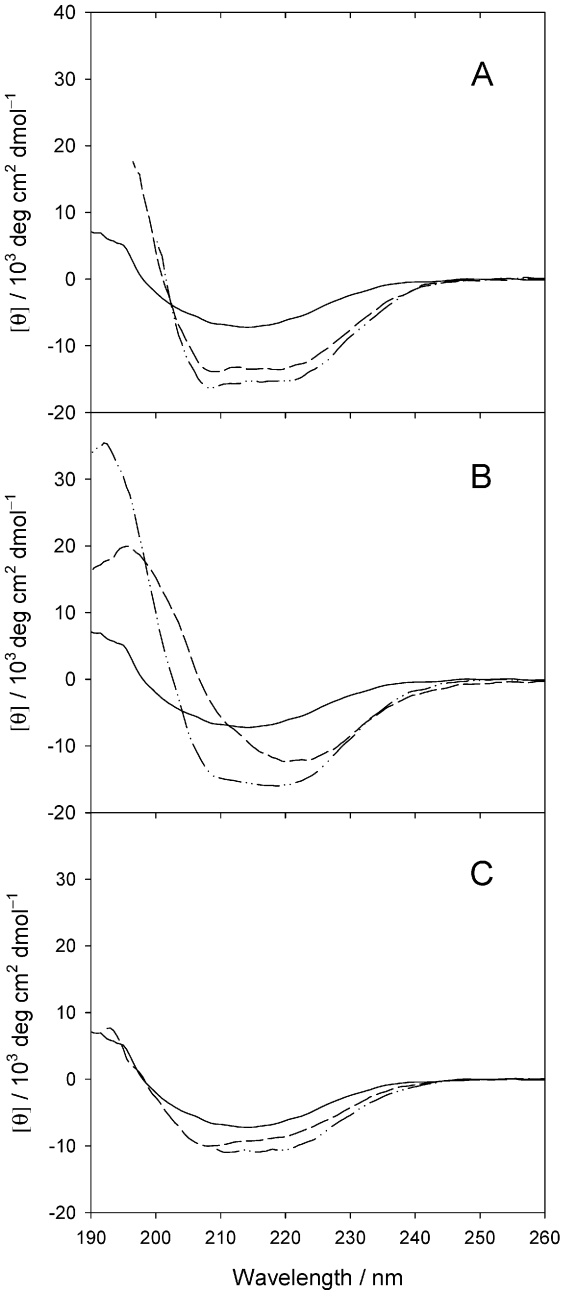

FIGURE 5: Structural changes of β-PrP with lipid membranes detected by CD. Far-UV CD spectra of β-PrP with POPG vesicles at pH 7 (A) at lipid-to-protein ratios of 500:1 (dashed line) and 1000:1 (dash-dot-dot line) and pH 5 (B) at lipid-to-protein ratios of 10:1 (dashed line) and 100:1 (dash-dot-dot line) and with DPPC/chol/SM vesicles (50:30:20, molar ratio) at pH 5 (C) at lipid-to-protein ratios of 100:1 (dashed line) and 500:1 (dash-dot-dot line). The spectrum of β-PrP alone is also shown in each panel (solid line).

PrP Aggregation and Fibril Formation in Lipid Membranes. Electron microscopy was employed to investigate the aggregation of PrP in lipid membranes. Electron micrographs of negatively stained α-PrP in solution at pH 5 show small uniformly dispersed aggregates, whereas at pH 7 larger aggregates are observed (Figure 7A,B). For α-PrP with POPC vesicles small round aggregates similar to those formed by α-PrP in solution were found (Figure 7C), consistent with the lack of binding of α-PrP to these vesicles (*26*). In contrast, extensive protein aggregation was observed

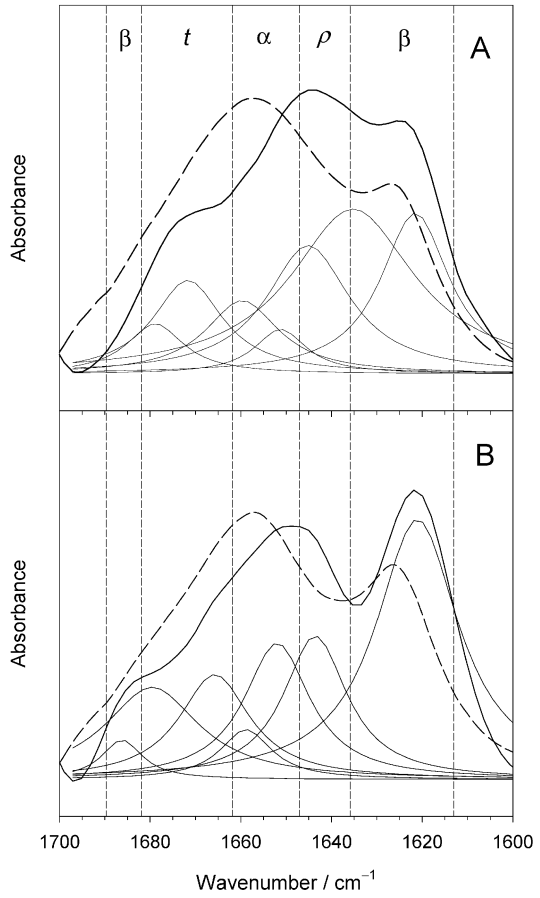

FIGURE 6: β-PrP unfolds in rafts and folds in POPG membranes. ATR FTIR of β-PrP with lipid rafts (A) and POPG membranes (B) in H_2O (dashed line) and after $H_2O/^2H_2O$ exchange (solid line). Vertical lines delimit the characteristic regions for various secondary structure elements: β-sheet (β), turns (t), α-helix (α), and random coil (ρ).

Table 1: Secondary Structure Content of PrP Isoforms in Solution and with Lipid Membranes Determined by ATR FTIR[a]

	secondary structure (%)				
system	α-helix	random coil	β-sheet	β-turns	others
α-PrP	37 (43)[b]	22 (21)[b]	9.5 (4)[b]	30 (32)[b]	1.5
β-PrP	21 (17)[c]	4 (5)[c]	35 (47)[c]	25 (31)[c]	13
β-PrP/POPG	19	15	43	23	0
β-PrP/raft	21	39	23	18	0
α-PrP/POPG	50	0	20	28	2
α-PrP/raft	—[d]	—[d]	—[d]	—[d]	—[d]

[a] The percentages represent the proportion of the total integrated intensity of the amide I bands identified by peak fitting (and confirmed by second derivative analysis when necessary) which have been assigned to the designated secondary structure components. ATR films were prepared from protein solutions or protein/lipid samples at pH 5 (see Experimental Procedures). [b] Values in parentheses represent the secondary structure content determined by NMR (*37*). [c] The secondary structure content of the proteinase K-resistant core of PrP extracted from tissues of diseased mammals is shown in parentheses (*2*). [d] No binding is observed for α-PrP with raft membranes at pH 5 (*26*).

for α-PrP with POPG both at pH 5 (Figure 7D) and at pH 7 (data not shown). In these preparations, protein aggregates were predominantly localized around the vesicles (Figure 7D). The EM analysis of α-PrP with DPPC/chol/SM membranes showed small round aggregates at pH 5 (Figure 7E), as seen for the protein in solution (Figure 7A) and with

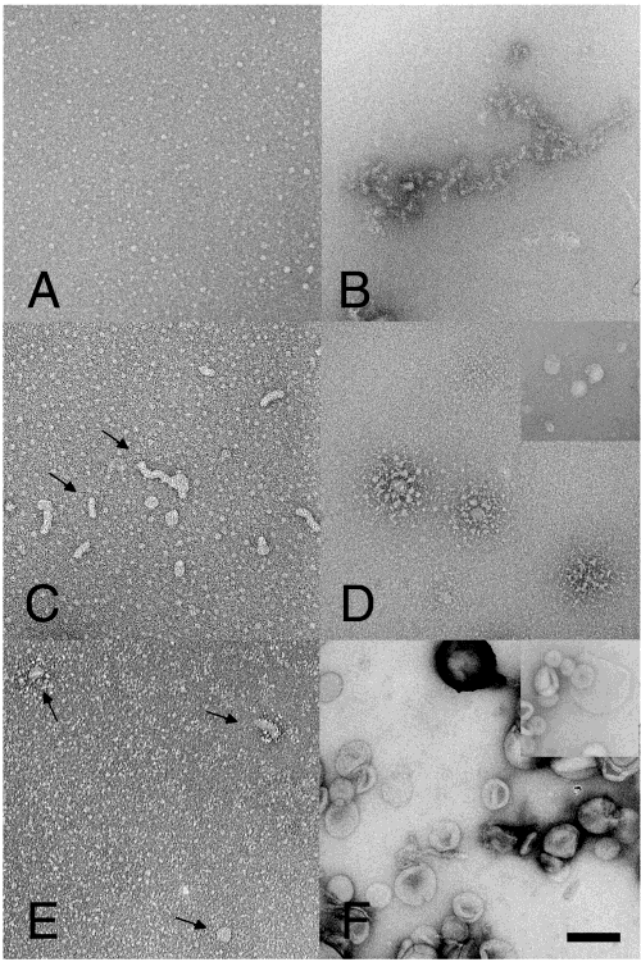

FIGURE 7: PrP aggregation in negatively charged lipid membranes. Electron micrographs of negatively stained α-PrP in solution at pH 5 (A) and pH 7 (B) and with lipid vesicles of POPC at pH 7 (C), POPG at pH 5 (D), and DPPC/chol/SM (50:30:20, molar ratio) at pH 5 (E) and pH 7 (F). Insets in panels D and F show corresponding lipid vesicles in the absence of PrP. Arrows in panels C and E are showing liposomes. Samples have a protein-to-lipid ratio of 1:176 (molar ratio). The bar scale is 100 nm.

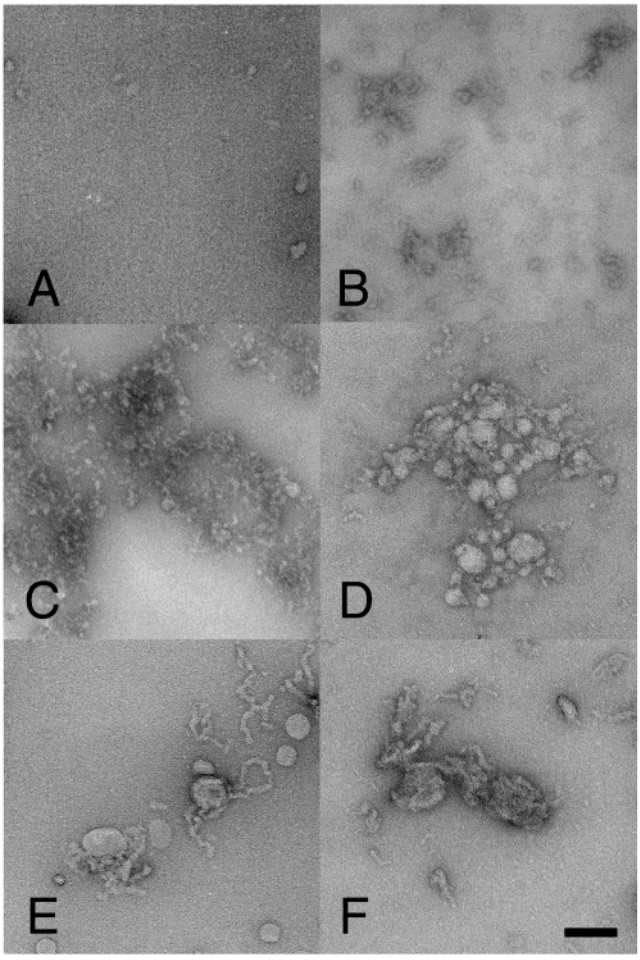

FIGURE 8: PrP fibrils are formed in raft-like membranes. Electron micrographs of negatively stained *β*-PrP in solution (A, B) and with lipid vesicles of POPG (C, D) and DPPC/chol/SM (50:30:20, molar ratio) (E, F) at pH 5 (A, C, E) and pH 7 (B, D, F). Samples have a protein-to-lipid ratio of 1:176 (molar ratio). The bar scale is 100 nm.

POPC membranes (Figure 7C). These observations are in good agreement with previous binding studies, where it was found that α-PrP does not bind to DPPC/chol/SM membranes at pH 5 (*26*). However, α-PrP binds to DPPC/chol/SM membranes at pH 7 (*26*), and the EM preparations show vesicles decorated with protein (Figure 7F).

EM of *β*-PrP with lipid membranes is presented in Figure 8. Small round aggregates are observed for *β*-PrP in solution at pH 5 (Figure 8A), and larger oblong aggregates are formed at pH 7 (Figure 8B). Preparations of *β*-PrP with POPC membranes showed diffused aggregates of protein in solution and lipid vesicles (data not shown), similar to the observations with α-PrP and POPC membranes shown in Figure 7C, and in agreement with the lack of binding of *β*-PrP to POPC membranes, as measured by Trp fluorescence. For the preparations of *β*-PrP with POPG membranes at pH 5 diffuse protein aggregates are observed, and it was difficult to find intact vesicles during EM analysis (Figure 8C). For *β*-PrP with POPG vesicles at pH 7, EM shows vesicles coated with protein, which seem to conglomerate into large aggregates (Figure 8D). Interestingly, for the preparations of *β*-PrP with raft membranes of DPPC/chol/SM, curvy and branched fibrillar structures were found around the lipid vesicles, particularly at pH 5 (Figure 8E).

DISCUSSION

It is thought that an interaction of PrP with the plasma membrane could play a role in the conversion of PrP^{C} into PrP^{Sc}. Supporting this hypothesis is the difference in sensitivity of PrP^{C} and PrP^{Sc} to treatment with the enzyme phosphatidylinositol-specific phospholipase C (PIPLC). Whereas PrP^{C} is easily cleaved upon treatment with PIPLC and removed from the membrane surface, PrP^{Sc} is retained on the membrane surface upon similar treatment (*13*, *14*). The results suggest that an altered association of PrP with lipid membranes may be an important factor in the molecular mechanism of prion conversion. However, very few studies have been devoted to the structural properties of prion protein associated with lipid membranes. In a previous study (*26*) we have characterized the binding of the α-helical isoform of PrP (α-PrP) to lipid membranes. In the current study, we investigate the binding of a *β*-sheet-rich form of PrP, designated *β*-PrP, to model lipid membranes. This *β*-sheet-enriched form of PrP has reduced cysteines (Cys 197 and 214) and upon oxidation (formation of disulfide bond) retains its *β*-sheet conformation (*5*). Scrapie PrP purified from brains

has been shown to contain an intramolecular disulfide bond (*51*, *52*). β-PrP occurs in a soluble oligomeric state, which tends to aggregate, as seen for PrP^{Sc}. Thus, *in vitro* refolded β-PrP may represent some of the properties of intermediate conformations of PrP that lead to PrP^{Sc}.

Trp fluorescence shows that β-PrP binds strongly to POPG membranes at pH 5 and less so at pH 7 (Figure 2). In contrast, α-PrP was shown to bind equally to POPG membranes at both pH 5 and pH 7 (*26*), with an affinity similar to that observed for the binding of β-PrP to POPG at pH 5 (Figure 1). The binding of PrP to POPG membranes is likely to be driven by strong electrostatic interactions between positively charged residues in the protein and the negatively charged lipid headgroup of POPG. At pH 5 PrP-(90−231) has a net charge of +9, whereas at pH 7 its net charge is +4. The observed differences in the binding of β-PrP to POPG membranes with pH corroborate the involvement of electrostatic interactions. However, the differences in binding properties observed for α-PrP and β-PrP with POPG membranes between pH 5 and pH 7 suggest that the β-isoform (β-PrP) may have a pH-dependent conformation. In fact, there are detectable differences in the spectroscopic properties of β-PrP between the two pH values. First, the fluorescence spectrum of β-PrP in solution at pH 7 has a λ_{max} shifted to lower wavelengths compared with the λ_{max} of β-PrP at pH 5, indicating a more buried environment for Trp residues. Second, the FTIR spectra of β-PrP at pH 7 and 5 show apparent differences (Figure 4), and spectral analysis revealed that β-PrP at pH 7 has less β-sheet structure (26%) and higher α-helix (34%) and random coil (14%) contents compared with β-PrP at pH 5 (Table 1). These results are consistent with the observed multiplicity of conformations for β-PrP isoforms *in vitro*, depending on refolding conditions (*6*, *8*).

As observed with α-PrP, β-PrP does not bind to POPC membranes at pH 7 or 5 (Figure 2). The α-helical isoform was found to bind to raft membranes at pH 7 but not at pH 5 (*26*). In contrast, in the current study we show that β-PrP binds to raft membranes at both pH 7 and pH 5. Like most GPI-anchored membrane proteins, PrP segregates into lipid rafts (also called ordered lipid domains) which are rich in lipids with saturated acyl chains, containing mainly phosphatidylcholine, cholesterol, and sphingomyelin (*18*, *19*). Mixed membranes composed of DPPC, cholesterol, and sphingomyelin have been shown to serve as good models of rafts (*38*). Therefore, it seems relevant that β-PrP binds to model raft membranes *in vitro*. Moreover, unlike α-PrP, β-PrP also binds to raft membranes at pH 5 as well as at pH 7. These results suggest that under the acidic conditions of endosomes the β-sheet isoform of PrP will have a higher affinity to lipid membranes than the α-helical isoform. In addition, the higher charge state of PrP at pH 5 leads to a more open structure than at pH 7, due to side chain charge repulsion on the protein surface. This more open structure exposes hydrophobic patches onto the protein surface, as demonstrated by ANS binding measurements (*39*), which would favor hydrophobic protein−lipid interactions. Thus, it is suggested that in endosomes PrP may have a higher propensity to stick to lipid membranes through a direct polypeptide−membrane interaction than at the surface of the plasma membrane where normally PrP is anchored via its GPI anchor.

Binding of β-PrP to lipid membranes results in significant structural changes in the protein. Far-UV CD spectra of β-PrP with POPG membranes show a clear transition from a spectrum with a broad minimum at ~218 nm, characteristic of β-sheet, for the protein in solution to spectra with defined minima at 208 and 222 nm (Figure 5A,B). These spectral changes indicate a structural transition from a protein conformation with a predominant β-sheet structure to a state richer in α-helical structure. For β-PrP with raft membranes smaller far-UV CD spectral changes are observed (Figure 5C). The FTIR spectra show that, generally, samples of β-PrP with POPG membranes have a narrower amide I band at ~1656 cm^{-1} and a well-defined component at ~1626 cm^{-1}, indicative of α-helix and β-sheet structure, respectively. In contrast, for β-PrP with raft membranes, the spectra show a broader amide I band at ~1656 cm^{-1}, which is associated with contributions from random coil (Figure 4). The combined results by far-UV CD and FTIR indicate an increase in α-helical structure for β-PrP with POPG membranes, whereas with raft membranes there is an increase in random coil. $H_2O/^2H_2O$ exchange measurements further corroborate this interpretation. ^2H_2O-exchanged spectra show a larger fraction of the amide I intensity shifted to wavenumbers associated with random coil for β-PrP with raft membranes (Figure 6A) in comparison with β-PrP with POPG membranes (Figure 6B). Peak fitting analysis of the amide I band showed that with POPG vesicles β-PrP retains its level of α-helical structure and gains random coil and β-sheet structure, whereas α-PrP acquires more α-helix and β-sheet using all random coil (Table 1). With raft membranes β-PrP also retains its level of α-helical structure, but a large fraction of β-sheet and turns are unfolded into random coil. In summary, POPG membranes appear to refold both α- and β-PrP, whereas raft membranes unfold β-PrP but induce α-helix in α-PrP.

Binding of β-PrP to negatively charged lipid membranes of POPG leads to total release of calcein from loaded vesicles (Figure 3), indicating a strong destabilization of the lipid bilayer. In contrast, raft vesicles retained their calcein contents upon binding of β-PrP (Figure 3). The effects are similar to those observed previously for the binding of α-PrP to POPG and raft membranes (*26*). Other studies have demonstrated that peptide or protein binding to lipid membranes can alter the bilayer integrity and/or permeability (*40*), either by forming pores in the membrane or by a detergent-like destabilization mechanism (*36*). Here, we show that the binding of β-PrP to negatively charged lipid membranes of POPG leads to a high perturbation in the integrity of the lipid bilayer resulting in total release of vesicle contents. Our results do not elucidate the molecular details of this PrP-induced membrane destabilization.

The precise mechanism of how PrP induces cell death is unclear, but *in vitro* studies have shown that peptides of PrP can be neurotoxic to cultured neurons (*41*, *42*). Various hypotheses have been postulated to explain neuronal cell death. These include increased oxidative stress as a result of depleted levels of PrP^{C} (*43*). Others have proposed a mechanism for prion neurotoxicity through a direct perturbation of the plasma membrane of nerve cells as a consequence of PrP^{Sc} accumulation (*44*, *45*). However, brain tissue devoid of PrP^{C} is not damaged by exogenous PrP^{Sc} (*46*). Strong aggregation of PrP in POPG membranes is associated with

high levels of calcein release, which suggests that aggregation of PrP strongly disrupts the integrity of the lipid bilayer. *In vivo*, such destabilization of the plasma membrane would lead to leakage of cytoplasmic contents and ultimately to cell death. Thus, our findings support previous studies that have proposed a mechanism for neurotoxicity through a direct interaction of PrP^{Sc} (or intermediate conformations on the pathway to PrP^{Sc}) with neuronal membranes.

We have suggested that the observed destabilization of POPG membranes upon binding of α-PrP could be related to the high β-sheet content of α-PrP bound to POPG, whereas the nondestabilizing effect on raft membranes could be associated with the increase in α-helix (*26*). A comparison of the level of β-sheet content in α-PrP with POPG membranes with that of β-PrP with raft membranes shows that α-PrP in POPG membranes has a similar amount of β-sheet to that of β-PrP in raft membranes (Table 1). Thus, the destabilizing effect of PrP to membranes is not directly correlated with their relative content in β-sheet structure. It is likely that other tertiary or quaternary structural properties may be responsible for the disruptive effect of PrP to membranes (see below).

Electron microscopy of samples incubated for up to 3 weeks reveals that preparations of α-PrP with POPG membranes accumulate amorphous aggregates of protein around the lipid vesicles (Figure 7D). In contrast, raft membranes appear to maintain their morphology with bound α-PrP, when compared with vesicles without protein (Figure 7F). The electron microscopy results of β-PrP show generally larger aggregates compared with preparations of α-PrP (Figures 7 and 8), consistent with the higher propensity of β-PrP to aggregate (*5*, *6*, *8*). Large amorphous aggregates concentrated around the lipid vesicles were observed for β-PrP with POPG vesicles at pH 7 (Figure 8D). In contrast, at pH 5 diffused protein aggregates were formed, which have the appearance of protofibrillar structures (Figure 8C). At pH 7 the protein appears to cluster several vesicles, whereas at pH 5 the vesicles are more dispersed and more difficult to find. Interestingly, for preparations of β-PrP with raft membranes at pH 5, fibrillar structures of PrP were formed (Figure 8E), and only amorphous aggregates at pH 7 could be found (Figure 8F). The fibrillar structures formed at pH 5 (Figure 8E) are not straight and long fibrils but are small, curvy, and branched, which is the typical appearance of protofibrils (*53*).

The precise subcellular compartment where PrP^{Sc} forms is unknown (*47*), but the current perception implicates the plasma membrane (*20*, *21*), lysosomes, and the endocytic pathway (*2*, *22*, *48*) as the most likely sites for PrP conversion. Our EM results show fibril formation for incubations of β-PrP with raft membrane at pH 5 and also some protofibrillar-like structures for β-PrP with POPG membranes, again at pH 5. Likewise, with membranes composed solely of negatively charged lipid, such as POPG, strong amorphous aggregation of PrP was observed. This aggregation may also result from the localized lower pH near the membrane surface of POPG membranes, due to the accumulation of protons by the negatively charged lipid headgroups (*49*). These acidic conditions at the membrane surface may also contribute to the observed tendency for increased β-sheet structure in POPG membranes, consistent with β-sheet isoforms of PrP being more favorably formed in acidic conditions (*6*, *8*, *50*). Thus, our combined results by FTIR and EM suggest that the acidic environment of lysosomes/endosomes may be more favorable for the conversion of PrP than the plasma membrane.

It is pertinent to correlate the EM results with calcein release from vesicles. Binding of both isoforms of PrP (α-PrP and β-PrP) to POPG membranes disrupts the integrity of the lipid bilayer, as measured by the release of calcein from loaded vesicles. The extent of release of vesicle contents was very similar for either α- or β-PrP at either pH, approaching 100% release of calcein (Figure 3). The EM images show extensive aggregation of PrP for all preparations with POPG vesicles (α- and β-PrP at pH 7 or 5). Thus, it seems that aggregation of PrP can be very disruptive to the integrity of lipid membranes. In contrast, raft membranes retain their vesicle contents upon binding of either α-PrP or β-PrP, and under EM these vesicles are easily found (Figures 7F and 8E). Interestingly, raft vesicles with β-PrP, which over time led to fibrillization of PrP, do not leak their calcein contents (Figure 3). This result indicates that the unfolded state of β-PrP associated with raft membranes does not disturb the integrity of the lipid bilayer. However, it should be emphasized that calcein release was monitored on freshly prepared vesicle−protein complexes. It remains to be investigated whether fibrillization of PrP in raft membranes induces leakage of vesicle contents, and this possibility is the subject of further studies.

In conclusion, our combined results by fluorescence, CD, FTIR, and EM show that β-PrP binds to POPG and raft membranes, both at pH 5 and at pH 7. Binding of β-PrP to POPG vesicles results in a membrane-associated state with a higher level of random coil and β-sheet structure, when compared with β-PrP in solution. This β-sheet-enriched form of β-PrP formed with POPG membranes destabilizes the lipid membrane, leading to total release of vesicle contents, and over time, amorphous aggregates of PrP form around the vesicles. Binding of β-PrP to raft membranes promotes a substantial unfolding of the protein. This membrane-associated more unfolded β-PrP does not destabilize the integrity of the lipid bilayer, and over time, preparations at pH 5 were found to contain fibrillar protein aggregates.

ACKNOWLEDGMENT

We thank Erik Goormaghtigh and Jean-Marie Ruysschaert (ULB, Brussels) for advice on ATR FTIR, Ken Davies (IAH, Compton) for AUC measurements on PrP isoforms, John Ellis (Warwick) for critical reading and comments on the manuscript, and Andrew Gill (IAH, Compton) for mass spectrometry of prion samples and insightful reading of the manuscript.

REFERENCES

1. Prusiner, S. B. (1998) *Proc. Natl. Acad. Sci. U.S.A. 95*, 13363−13383.
2. Caughey, B. W., Dong, A., Bhat, K. S., Ernst, D., Hayes, S. F., and Caughey, W. S. (1991) *Biochemistry 30*, 7672−7680.
3. Pan, K. M., Baldwin, M. A., Nguyen, J., Gasset, M., Servban, A., Groth, D., Mehlhorn, I., Huang, Z., Fletterick, R. J., Cohen, F. E., and Prusiner, S. B. (1993) *Proc. Natl. Acad. Sci. U.S.A. 90*, 10962−10966.
4. Caughey, B., Raymond, G. J., Callahan, M. A., Wong, C., Baron, G. S., and Xiong, L.-W. (2001) *Adv. Protein Chem. 57*, 139−169.

5. Zhang, H., Stöckel, J., Mehlhorn, I., Groth, D., Baldwin, M. A., Prusiner, S. B., James, T. L., and Cohen, F. E. (1997) *Biochemistry 36*, 3543−3553.
6. Lu, B.-Y., and Chang, J.-Y. (2001) *Biochemistry 40*, 13390−13396.
7. Swietnicki, W., Morillas, M., Chen, S. G., Gambetti, P., and Surewicz, W. K. (2000) *Biochemistry 39*, 424−431.
8. Baskakov, I. V., Legname, G., Baldwin, M. A., Prusiner, S. B., and Cohen, F. E. (2002) *J. Biol. Chem. 277*, 21140−21148.
9. Jackson, G. S., Hosszu, L. L. P., Power, A., Hill, A. F., Kenney, J., Saibil, H., Craven, C. J., Waltho, J. P., Clarke, A. R., and Collinge, J. (1999) *Science 283*, 1935−1937.
10. Morillas, M., Vanik, D. L., and Surewicz, W. K. (2001) *Biochemistry 40*, 6982−6987.
11. Jansen K., Schafer, O., Birkmann, E., Post, K., Serban H., Prusiner, S. B., and Riesner, D. (2001) *Biol. Chem. 382*, 683−691.
12. Gabizon, R., McKinley, M. P., and Prusiner, S. B. (1987) *Proc. Natl. Acad. Sci. U.S.A. 84*, 4017−4021.
13. Stahl, N., Borchelt, D. R., and Prusiner, S. B. (1990) *Biochemistry 29*, 5405−5412.
14. Safar, J., Ceroni, M., Gajdusek, D. C., and Gibbs, C. J. (1991) *J. Infect. Dis. 163*, 488−494.
15. Lehmann, S., and Harris, D. A. (1995) *J. Biol. Chem. 270*, 24589−24597.
16. Hay, B., Prusiner, S. B., and Lingappa, V. R. (1987) *Biochemistry 26*, 8110−8115.
17. Stahl, N., Borchelt, D. R., Hsiao, K., and Prusiner, S. B. (1987) *Cell 51*, 229−240.
18. Vey, M., Pilkuhn, S., Wille, H., Nixon, R., DeArmond, S. J., Smart, E. J., Anderson, R. G. W., Taraboulos, A., and Prusiner, S. B. (1996) *Proc. Natl. Acad. Sci. U.S.A. 93*, 14945−14949.
19. Naslavsky, N., Stein, R., Yanai, A., Friedlander, G., and Taraboulos, A. (1997) *J. Biol. Chem. 272*, 6324−6331.
20. Caughey, B., and Raymond, G. J. (1991) *J. Biol. Chem. 266*, 18217−18224.
21. Taraboulos, A., Scott, M., Semenov, A., Avraham, D., Laszlo, L., and Prusiner, S. B. (1995) *J. Cell Biol. 129*, 121−132.
22. Baron, G. S., Wehrly, K., Dorward, D. W., Chesebro, B., and Caughey, B. (2002) *EMBO J. 21*, 1031−1040.
23. Caughey, B. (1991) *Sem. Virol. 2*, 189−196.
24. Shyng, S.-L., Huber, M. T., and Harris, D. A. (1993) *J. Biol. Chem. 268*, 15922−15928.
25. DeArmond, S. J., and Prusiner, S. B. (1995) *Am. J. Pathol. 146*, 785−811.
26. Sanghera, N., and Pinheiro, T. J. T. (2002) *J. Mol. Biol. 315*, 1241−1256.
27. Mehlhorn, I., Groth, D., Stockel, J., Moffat, B., Reilly, D., Yansura, D., Willett, W. C., Baldwin, M., Fletterick, R., Cohen, F. E., Vandlen, R., Henner, D., and Prusiner, S. B. (1996) *Biochemistry 35*, 5528−5537.
28. Gill, S. C., and Hippel, P. H. (1989) *Anal. Biochem. 182*, 319−326.
29. Rankin, S. E., Watts, A., and Pinheiro, T. J. T. (1998) *Biochemistry 37*, 12588−12595.
30. Fringeli, U. P., and Günthard, H. H. (1981) *Mol. Biol. Biochem. Biophys. 31*, 270−332.
31. Goormaghtigh, E., Cabiaux, V., and Ruysschaert, J.-M. (1990) *Eur. J. Biochem. 193*, 409−420.
32. Raussens, V., Ruysschaert, J.-M., and Goormaghtigh, E. (1997) *J. Biol. Chem. 272*, 262−270.
33. Cabiaux, V., Brasseur, R., Wattiez, R., Falmagne, P., Ruysschaert, J.-M., and Goormaghtigh, E. (1989) *J. Biol. Chem. 264*, 4928−4938.
34. Defrise-Quertain, F., Cabiuax, V., Vandenbranden, M., Wattiez, R., Falmagne, P., and Ruysschaert, J.-M. (1989) *Biochemistry 28*, 3406−3413.
35. Butko, P., Huang, F., Pusztai-Carey, M., and Surewicz, W. K. (1996) *Biochemistry 35*, 11355−11360.
36. Vogt, T. C. B., and Bechinger, B. (1999) *J. Mol. Biol. 274*, 29115−29121.
37. James, T. L., Liu, H., Ulyanov, N. B., Farr-Jones, S., Zhang, H., Donne, D. G., Kaneko, K., Groth, D., Mehlhorn, I., Prusiner, S. B., and Cohen, F. E. (1997) *Proc. Natl. Acad. Sci. U.S.A. 94*, 10086−10091.
38. Schroeder, R., London, E., and Brown, D. (1994) *Proc. Natl. Acad. Sci. U.S.A. 91*, 12130−12134.
39. Swietnicki, W., Petersen, R. B., Gambetti, P., and Surewicz, W. K. (1997) *Biol. Chem. 272*, 27517−27520.
40. White, S. H., and Wimley, W. C. (1994) *Curr. Opin. Struct. Biol. 4*, 79−86.
41. Forloni, G., Angeretti, N., Chiesa, R., Monzani, E., Salmona, M., Bugiani, O., and Tagliavini, F. (1993) *Nature 362*, 543−546.
42. Brown, D. R., Schmidt, B., and Kretzschmar, H. A. (1996) *Nature 380*, 345−347.
43. Brown, D. R., Schulz-Schaeffer, W. J., Schmidt, B., and Kretzschmar, H. A. (1997) *Exp. Neurol. 146*, 104−112.
44. Pillot, T., Lins, L., Goethals, M., Vanloo, B., Baert, J., Vandekerckhove, J., Rosseneu, M., and Brasseur, R. (1997) *J. Mol. Biol. 274*, 381−393.
45. Lin, M.-C., Mirzabekov, T., and Kagan, B. L. (1997) *J. Biol. Chem. 272*, 44−47.
46. Brandner, S., Isenmann, S., Raeber, A., Fischer, M., Sailer, A., Kobayashi, Y., Marino, S., Weissmann, C., and Aguzzi, A. (1996) *Nature 379*, 339−343.
47. Caughey, B. (2001) *Trends Biochem. Sci. 26*, 235−242.
48. Borchelt, D. R., Taraboulos, A., and Prusiner, S. B. (1992) *J. Biol. Chem. 267*, 16188−16199.
49. Prats, M., Teissié, J., and Toccane, J. F. (1986) *Nature 322*, 756−758.
50. Hornemann, S., and Glockshuber, R. (1998) *Proc. Natl. Acad. Sci. U.S.A. 95*, 6010−6014.
51. Turk, E., Teplow, D. B., Hood, L. E., and Prusiner S. B. (1988) *Eur. J. Biochem. 176*, 21−30.
52. Welker, E., Raymond, L. D., Scheraga, H. A., and Caughey, B. (2002) *J. Biol. Chem. 277*, 33477−33481.
53. Harper, J. D., Wong, S. S., Lieber, C. M., and Lansbury, P. T. (1999) *Biochemistry 38*, 8972−8980.

BI026872Q